

Effects of Defect on Work Function and Energy Alignment of PbI₂: Implications for Solar Cell Applications

Hongfei Chen[§], Hejin Yan[§], Yongqing Cai^{§*}

[§] Joint Key Laboratory of the Ministry of Education, Institute of Applied Physics and Materials Engineering, University of Macau, Taipa, Macau, China

ABSTRACT

Two-dimensional (2D) layered lead iodide (PbI₂) is an important precursor and common residual species during the synthesis of lead-halide perovskites. There currently exist some debates and uncertainties about the effect of excess PbI₂ on the efficiency and stability of the solar cell with respect to its energy alignment and energetics of defects. Herein, by applying the first-principles calculations, we investigate the energetics, changes of work function and the defective levels associated with the iodine vacancy (V_I) and interstitial iodine (I_I) defects of monolayer PbI₂ (ML-PbI₂). We find that the PbI₂ has a very low formation energy of V_I of 0.77 and 0.19 eV for dilute and high concentration, respectively, reflecting coalescence tendency of isolated V_I, much lower than that of vacancies in other 2D materials like phosphorene. Similar to V_I, a low formation energy of I_I of 0.65 eV is found, implying a high population of such defects. Both defects generate in-gap defective levels which are mainly due to the unsaturated chemical bonds of *p*-orbitals of exposed Pb or inserted I. Such rich defective levels allow the V_I and I_I as the reservoir or sinks of electron/hole carriers in PbI₂. Our results suggest that the remnant PbI₂ in perovskite MAPbI₃ (or FAPbI₃) would play dual opposite roles in affecting the efficiency of the perovskite: (1) Forming Schottky-type interface with MAPbI₃ (or FAPbI₃) in which the built-in potential would facilitate the electron-hole separation and prolong the carrier lifetime; (2) Acting as the recombination centers due to the deep defective levels. To promote the efficiency by the Schottky effect, our work reveals that the I_I defect is favored, and to reduce the recombination centers the V_I defect should be suppressed. Our results provide a deep

understanding of the effects of defect-engineering in ML-PbI₂, which shall be beneficial in improving strategies for the related optoelectronics applications.

Introduction

Hybrid organic-inorganic perovskite materials have recently attracted widespread attention in photoelectric fields due to their superior features of high absorption coefficients¹, desirable optical band gaps², long carrier lifetime and diffusion length³. Specifically, the power conversion efficiency (PCE) of perovskite solar cells (PSCs) has reached ~25.5%⁴, while the key to realizing a good performance of PSCs is indispensable with the uniform and well-crystallized perovskite absorbed films⁵. During the one-step reaction, changing the stoichiometry of the precursors PbI_2 provides a simple means of varying the chemical potential and the outcome of the reaction, including the defect concentration, doping, and final composition⁶. In two-step synthesis methods, the lead iodide (PbI_2) film is deposited and subsequently exposed to solutions of the organic salts thus obtaining the perovskite thin films after thermal annealing^{7, 8}. However, the PbI_2 in the bottom layer cannot completely interpenetrate with the organic solution in the upper layer, resulting in uncontrollable PbI_2 residue. The reaction process in solution proceeds by topotactic nucleation followed by grain growth by dissolution–reconstruction. There is a strong orientational and structural relationship between the final stage of the solution-reacted MAPbI_3 product and the initial PbI_2 crystallite⁹⁻¹¹. As the precursor material used to fabricate perovskite thin films^{12, 13}, PbI_2 is critical for efficient PCE due to the $6s^2$ electronic configuration of Pb atoms¹⁴. More notably, a slight excess of PbI_2 in the perovskite film has been observed to be beneficial¹⁵⁻¹⁸. The remnant PbI_2 , randomly distribute in the perovskite layer, on the surface or the grain boundary, can suppress charge recombination and reduce the intrinsic halide vacancy concentration thereby passivate trap states^{8, 15, 19-22}. It was also theoretically confirmed that the slight excess PbI_2 is able to reduce surface cation concentration and the corresponding nonadiabatic coupling decreased by one order of magnitude, hence the charge carrier lifetime extended²³. However, the excess/unreacted PbI_2 will decompose into lead and iodine under illumination, which trigger and accelerate the degradation of PSCs²⁴.

Actually, PbI_2 , with layered crystalline structure composed of covalently bonded I–Pb–I atomic planes, is a promising candidate as two-dimensional (2D) semiconductor material owing to its superior optoelectronic properties²⁵⁻²⁷. The 2H phase is the most thermal stable structure for bulk PbI_2 at room temperature²⁸, but the stacking forms of the adjacent $(\text{I–Pb–I})_n$ layers are

diverse due to the weak van der Waals interactions^{29, 30}. In contrast to other layered semiconductors like MoS₂ and WS₂, which prefer to n-type behavior, the PbI₂ tends to have a p-type feature with tunable bandgap which strongly depends on the thickness³¹⁻³³. As theoretical and experimental researches shown, the band structure of PbI₂ would change from a direct bandgap of ~2.38 eV to an indirect bandgap of ~2.5 eV as the thickness decrease from bulk to monolayer^{27, 34, 35}. These unique properties trigger many studies on the growth, exfoliation, and applications of the PbI₂ nanostructure^{34, 36-40} in optoelectronic devices, photodetectors, and photon detection⁴¹⁻⁴³. In this work, we prefer to focus on monolayer-PbI₂ (ML-PbI₂), according to the following reasons: (1) The evidence for the ML-PbI₂ has been discovered by electrocrystallisation⁴⁴ and the crystalline state of PbI₂ has the hexagonal CdI₂ type structure. (2) The excess PbI₂ species are distributed as nanosheets between the grain boundaries of the perovskite film^{20, 45}. (3) In 2D PbI₂, low dimensionality provides a sensitive conductive channel for carriers and reduces phonon thermal transport at the same time⁴⁶. (4) Moreover, it is possible to fabricate ML-PbI₂ with other 2D materials, such as graphene, by epitaxial growth and layer-control in photovoltaic and thermoelectric systems^{39, 47, 48}.

Point defects, which are probably to be unintentionally introduced during fabrication and applications, are common in high specific surface area 2D materials. Besides, it is known that defective states, which are situated within the bandgap, affect dramatically carrier mobility and photocatalysis of 2D material. Such defective states can tune band gaps for enhancing light absorption, act as active sites for separating photogenerated carriers, and serve in molecular chemical adsorption with significantly decreased energy barrier of reactions^{47, 49-51}. In previous studies, volatile species (for example I₂) were found to rapidly decompose perovskites to causes severe degradation^{52, 53}. Besides, single-point iodine vacancy (V_I) of sublattice sites in ML-PbI₂ has also been observed in the previous experiments⁴⁸. Related properties of ML-PbI₂ with V_I and nonmetallic atoms doping were theoretically investigated⁵⁴. The results pointed that spin-orbit coupling (SOC) does not alter the electron occupation of the bands near the Fermi level. However, the effect of V_I, in particularly its concentration, and interstitial iodine (I_I) on ML-PbI₂ remains unexplored. Considering the prominent role of PbI₂ in organic-inorganic perovskite, further understanding of the defect mechanisms of ML-PbI₂ that are predominantly involved with V_I and I_I is thus critically important for practical applications.

In this work, we explored the energetics, changes of work function, and the electronic properties of the pristine ML-PbI₂, defective levels associated with the V_I in different concentrations and I_I in two interacted sites by first-principles calculations. Our calculations reveal that the ML-PbI₂ has a relatively low formation energy of V_I and I_I, implying a high population of such defects under thermodynamic equilibrium conditions. Moreover, the in-gap defective levels in both V_I and I_I allow the reservoir or sinks of electron/hole carriers in PbI₂. It is suggested that the remnant PbI₂ in perovskite MAPbI₃ (or FAPbI₃) would play dual opposite roles of the perovskite: (1) Forming Schottky-type interface with MAPbI₃ (or FAPbI₃) in which the built-in potential would facilitate the electron-hole separation and prolong the carrier lifetime; (2) Acting as the recombination centers due to the deep defective levels. The I_I is favored in order to promote the efficiency by the Schottky effect, and the V_I would be suppressed for reducing the recombination centers.

Method

The theoretical calculations were performed using density functional theory (DFT) method as implemented in the Vienna ab initio simulation package (VASP)^{55, 56}. The generalized gradient approximation (GGA) of Perdew–Burke–Ernzerhof (PBE) exchange-correlation functional was adopted for geometry optimization and electronic properties^{57, 58}, and the Heyd–Scuseria–Ernzerhof (HSE06) functional⁵⁹ was further employed in the density of state (DOS) and band structure calculations for describing the electronic interactions more precisely. The plane wave basis was applied with a kinetic cutoff energy of 300 eV. The Brillouin zone was sampled with a 2×2×1 and a 1×1×1 Gamma centered Monkhorst-Pack grids for PBE and HSE calculations, respectively. The dispersion correction of DFT-D3 was also considered⁶⁰. All structures were fully relaxed under the convergent criterion of 0.01 eVÅ⁻¹ for atomic force. The relaxed lattice constant of PbI₂ unit cell is $a = b = 4.593$ Å, which is in good agreement with the experiment result (4.557 Å)³⁴. Meanwhile, a larger 6×6×1 supercell (36 Pb atoms and 72 I atoms contained) of ML-PbI₂ was also considered. An 18 Å vacuum space was added on the z direction to eliminate the effect of image atoms. The work function W is calculated via the formula:

$$W = E_{vac} - E_F \quad (1)$$

where E_{vac} is the energy in vacuum level, and E_F is the Fermi energy. The band diagram of defect states is aligned through calibrating E_{vac} .

Formation energy E_f of defects in ML-PbI₂ per single V_I or single I_I was calculated as:

$$E_f = \frac{1}{n} [E_{tot}(Pb_{36}I_{72+n}) - E_{tot}(Pb_{36}I_{72}) - \sum n\mu_I] \quad (2)$$

where $E_{tot}(Pb_{36}I_{72+n})$ is total energy of the ML-PbI₂ supercell with vacancies or interstitials, $E_{tot}(Pb_{36}I_{72})$ is the total energy of prinstic ML-PbI₂, n is the number of I atoms that have been added ($n > 0$) to or removed ($n < 0$) from the supercell when the V_I or I_I doping is introduced, and μ_I is the chemical potentials. The value of the μ_I of I is defined within the range of values corresponding to Pb-rich or I-rich conditions. Under I-rich condition, the μ_I is equal to the energy of a I atom in a I₂ molecule. Under Pb-rich condition, μ_I is determined as half of the energy difference between one formula unit of supercell ML-PbI₂ and a Pb atom in bulk.

Results and discussion

The original 1T phase ML-PbI₂ nanosheet, obtained from the 2H-PbI₂ bulk²⁸, has a hexagonal structure with space group $P\bar{3}m1$. Its atomic structure is similar to the 1T-TMDs (MoS₂ and WS₂), where the atomic plane of Pb is enclosed by two nonaligned I atomic layers to form the ABC stacking pattern, each Pb atom connects with six nearest I atoms forming an octahedral coordination unit [PbI₆]⁴⁻. The optimized lattice constant and thickness of single layer PbI₂ are 4.59 Å and 3.78 Å, respectively. The averaged interatomic distance of Pb-I is 3.27 Å, which shows good agreement with the experimental value (3.24 Å)^{35, 36}.

The defect states including the V_I and I_I are schematically shown in Fig. 1. The insets show the top and side views of the optimized defective states, corresponding to: (a) I_I near the I atom in the basal plane (denoted as I_{I-1}), (b) I_I above the Pb atom (denoted as I_{I-Pb}), (c) V_I. We have considered both the diluted V_I with concentration of 1.38% (denoted as V_{I-1}) and more concentrated vacancies with content of 9.72% (V_{I-2}) and 19.44% (V_{I-3}) for simulating the PbI₂ with low, medium and high concentrations, respectively. Such iodine deficiencies are highly likely to exist in remnant PbI₂ during the reactions from PbI₂ to perovskite PSCs. Although there exist ionic component during the synthesis, the neutral charge state seems relatively stable at a large range of chemical potential^{48, 61}, so we mainly concentrate on the stability of diluted

defects on neutral charge states. For the latter two cases, the vacancies are modelled by removing iodine atoms randomly and uniformly at the top and bottom iodine layers (see more information in Fig. S1 and S2 in supporting information). Since the PbI_2 lattice has relatively big void and may uptake some iodine atoms, we have also considered the possibility of the I_i atom located within the sheet of I-Pb-I atomic layer. However, the optimized structure is quite similar to the situation of $\text{I}_{\text{I-I}}$ owing to the repulsion from hosted atoms. Moreover, the coexistence of vacancy-interstitial (V-I) pairs is also discussed by employing the climbing image nudged elastic band (NEB) method. This kind of Frenkel defects is common in 2D materials and extensively discussed, like in black phosphorus⁶². The energy profiles corresponding to the formation and recombination of V-I pairs are shown in Fig. S3 and S4. We found that the V-I pairs are prone to interact or recombine if concentrations are high.

The formation energies E_f are calculated and listed in Table 1. At finite temperature T , the defect population is exponentially related to E_f according to the Boltzmann distribution. The average equilibrium concentrations defects in ML- PbI_2 can be estimated by using $n/N = \exp(-\Delta E/k_B T)$, where n is the number of defects, N is the total number of atomic sites in PbI_2 , k_B is the Boltzmann constant, and ΔE is the formation energy with a value of 0.77 eV for $\text{V}_{\text{I-I}}$, 0.68 eV for $\text{I}_{\text{I-I}}$ and that of 0.65 eV for $\text{I}_{\text{I-Pb}}$. The thermodynamic equilibrium concentrations of $\text{V}_{\text{I-I}}$ ($\sim 10^{-13} \text{ cm}^{-2}$), $\text{I}_{\text{I-I}}$ and $\text{I}_{\text{I-Pb}}$ ($\sim 10^{-12} \text{ cm}^{-2}$) are low at room temperature, however their concentrations would increase rapidly with increasing temperature. Moreover, high concentrations of defects can also be achieved by irradiation, which is a well-accepted approach for the introduction and control of defects.

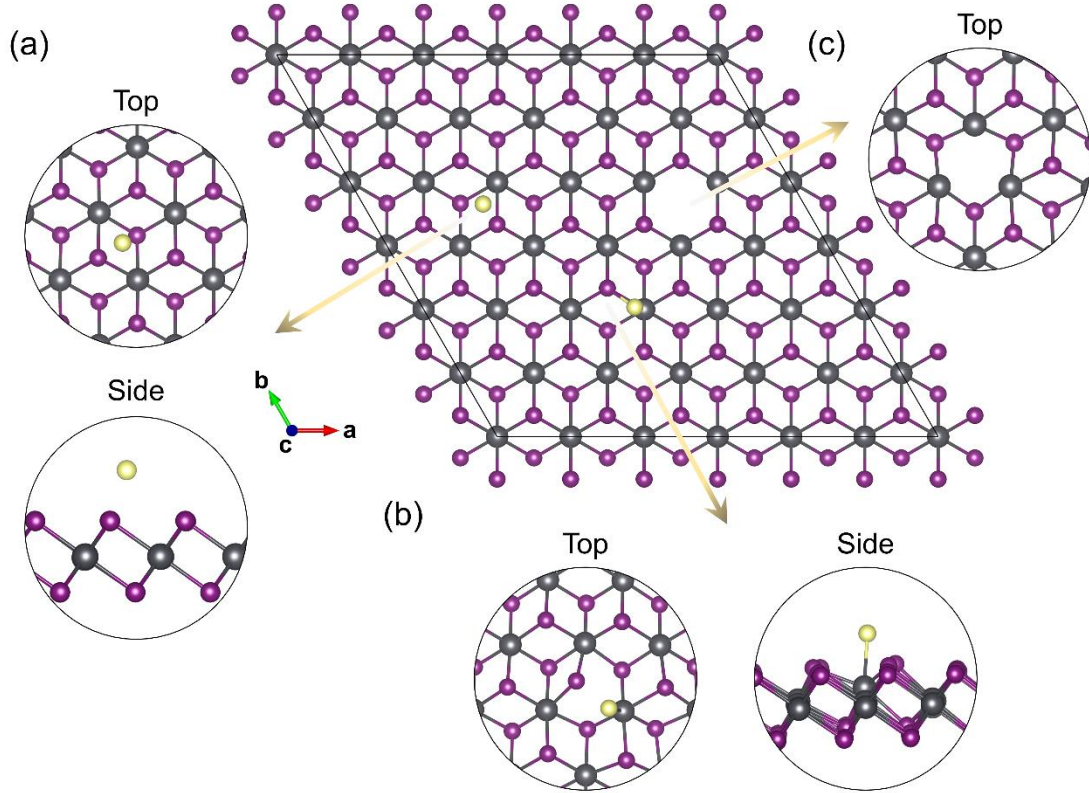


Figure 1. Top view of ML-PbI₂ 6×6×1 supercell with schematically assembled unrelaxed defective structures of isolated V_I and I_I. The dark gray balls represent Pb atoms, the purple balls represent I atoms and the yellow balls represent the interstitial I atoms. The insets show the top and side views of each relaxed configurations of (a) I_{I-I}, (b) I_{I-Pb} and (c) V_{I-I}.

Pristine ML-PbI₂:

At first, the electronic properties of the perfect ML-PbI₂ and corresponding Pb-I bonding mechanism were investigated. It is well known that the standard PBE functional underestimates the band gap (E_g) of monolayer PbI₂, and more precise band structure and E_g can be corrected by the hybrid functional. The calculated results of the ML-PbI₂ band structure are displayed in Fig. 2a and b. The E_g is 2.55 eV for PBE, which is in good agreement with previously DFT result (2.57 eV)^{35, 46}. In addition, this value changes when using the more reliable HSE06 functional with the E_g increases to 3.32 eV. The overall shape of the valence and conduction bands of pristine ML-PbI₂ is similar for both PBE and HSE methods of calculation. For ML-PbI₂, the conduction band minimum (CBM) is located at Γ point, while the valence band maximum (VBM) is situated at the K point. There presents an energy difference between the

direct bandgap at the Γ point and the indirect bandgap (VBM at the K point and CBM at the Γ point) of 0.02 eV in PBE results, while 0.04 eV in HSE results. This direct (bulk PbI_2) to indirect (ML- PbI_2) transition is mainly originated from the elimination of van der Waals interaction. We find the anti-orbital hybridization between the 5p orbitals of I atoms and 5s orbitals of Pb atoms plays an essential role in this phenomenon.

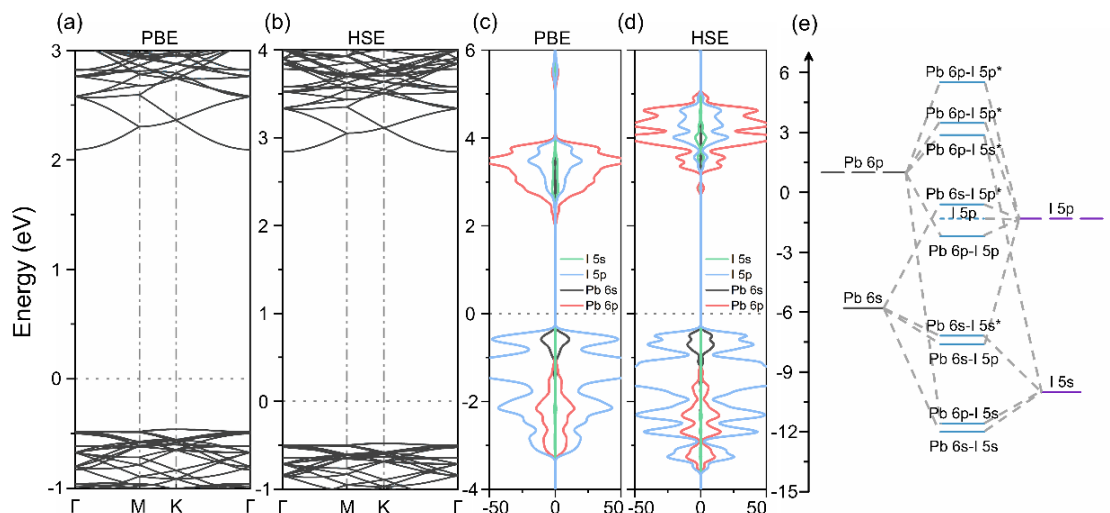


Figure 2. Band structure of pristine ML- PbI_2 by (a) PBE and (b) HSE methods. PDOS of pristine ML- PbI_2 by PBE (c) and HSE (d). In (c) and (d), the Pb-6s, Pb-6p, I-5s and I-5p states are represented by black, red, green and blue lines, respectively. (e) Diagram of molecular orbital hybridization between Pb and I atoms analyzed from (a). The Fermi level is set at zero, the blue dashed line in (e) represents the nonbonding I 5p states.

Figure 2c and d show the projected density of state (PDOS) of pristine ML- PbI_2 using PBE and HSE methods, respectively. The number of valence electrons (atomic orbitals) explicitly treated is 14 for Pb ($5d^{10}6s^26p^2$) and 7 for I ($5s^25p^5$). It should be noted that the Pb 5d subshell is full and not involved in the bonding thus not analyzed. According to the orbital decomposition analysis of the PBE band structure (Fig. 2a), the Pb 6p orbitals dominate the CBM, while the I 5p orbitals and Pb 6s orbitals mainly contribute to the VBM. Figure 2e shows the orbital hybridization between Pb and I atoms, which well reveals the bonding state of PbI_2 . The valence bands (VBs) near the Fermi level are composed of Pb (6s)-I (5p) antibonding states (-1.10 ~ -0.38 eV), I (5p) nonbonding states (~ -1.32 eV), and Pb (6p)-I (5p) bonding

states (-3.29 ~ -1.10 eV). Some other bonding or hybridized states are found below the top broad VBs, but too deep and thus less contributing to the physical/chemical processes. Specifically, the Pb (6s)-I (5s) antibonding states are formed within 0.87 eV (-7.80 ~ -6.93 eV), while in the deeper position of this range the Pb (6s)-I (5p) hybridized states are detected (The larger energy scale for Fig. 2c shows in Fig. S5). The lowest energy bands are Pb (6p)-I (5s) and Pb (6s)-I (5s) weak bonding states (-12.29 ~ -11.32 eV). For the conduction bands (CBs), the weak Pb (6p)-I (5s) antibonding states and strong Pb (6p)-I (5p) antibonding states (2.08 eV ~ 4.01 eV) are observed above the Fermi level. We also compare the defective levels of different charged states (-1, 0, +1) of V_{I-1} and I_{I-Pb} defects aligned to vacuum level (Fig. S6) and there are some variations of the positions of the positions.

Iodine vacancies

The intrinsic defects, like atomic vacancies are inevitably introduced in PbI_2 during the preparation processes. The doping of vacancies has a great influence on the electronic properties, such as enhancing light absorption for photocatalyst, acting as molecular adsorption sites and channels for electrons and holes transfer^{63, 64}. Here, we investigated the effect of various V_I (V_{I-1} , V_{I-2} , V_{I-3}) corresponding to the concentrations of 1.38%, 9.72%, and 19.44% on the structural and electronic properties of ML- PbI_2 . The formation energies E_f are calculated and listed in Table 1. The E_f of all the V_I are positive under both Pb-rich and I-rich conditions implying endothermic processes and additional energy is required for the vacancy production. As expected the V_I under Pb-rich condition has a lower E_f than that under I-rich condition, indicating that V_I is more prone to form under Pb-rich condition. Under dilute doping, the E_f of V_{I-1} ranges from 0.77 eV (Pb-rich condition) to 2.65 eV (I-rich condition). The value is even smaller than those of phosphorus vacancy in phosphorene (1.65 eV), V_S in MoS_2 (from 1.22 to 2.25 eV), V_N (from 4.90 to 7.60 eV) and V_B (from 7.50 to 10.20 eV) in h -BN⁶⁵. This ultralow E_f in PbI_2 suggests a very weak Pb-I bond and facile introduction of isolated V_I in PbI_2 .

Surprisingly, when more vacancies are introduced in the PbI_2 sheet, the E_f can be further reduced. For the medium-level concentrated V_{I-2} and highly concentrated V_{I-3} , the E_f decreases from that of the single V_I under both Pb-rich and I-rich conditions: V_{I-2} (from 0.50 to 2.39 eV) and V_{I-3} (from 0.19 to 2.08 eV). This implies that V_I tends to couple with each other and form

vacancy clusters.

Figure 1c shows the relaxed structure of single vacancy (V_{I-1}). Isolated V_I creates three exposed Pb atoms which exhibit an inward relaxation by moving toward the center of the V_I , while the nearest neighbour (NN) iodine atoms show an outward relaxation since the distortion of Pb-I bonds. The loss of an I atom in the PbI_2 sheet creates three dangling bonds associated with the unpaired atoms of the three NN Pb atoms. The Pb-I bond length between the first-NN Pb atoms and the next-NN I atoms to the V_I is shortened from 3.27 Å to 3.21 Å. When the concentration increases from V_{I-1} , V_{I-2} to V_{I-3} , the lattice constants of $6 \times 6 \times 1$ PbI_2 supercell decrease from 27.56, 27.26 to 25.23 Å, respectively, reflecting a shrinkage of the lattice for structures with significant iodine deficiency.

Table 1

The formation energy E_f of V_I and I_I ML- PbI_2 under Pb-rich and I-rich conditions. The work function W calculated by the difference of vacuum level energy and Fermi energy.

System	E_f (eV)		W (eV)
	Pb-rich	I-rich	
perfect	0	0	5.91
V_{I-1}	0.77	2.65	5.58
V_{I-2}	0.50	2.39	5.76
V_{I-3}	0.19	2.08	4.60
I_{I-1}	2.56	0.68	4.62
I_{I-Pb}	2.54	0.65	4.62

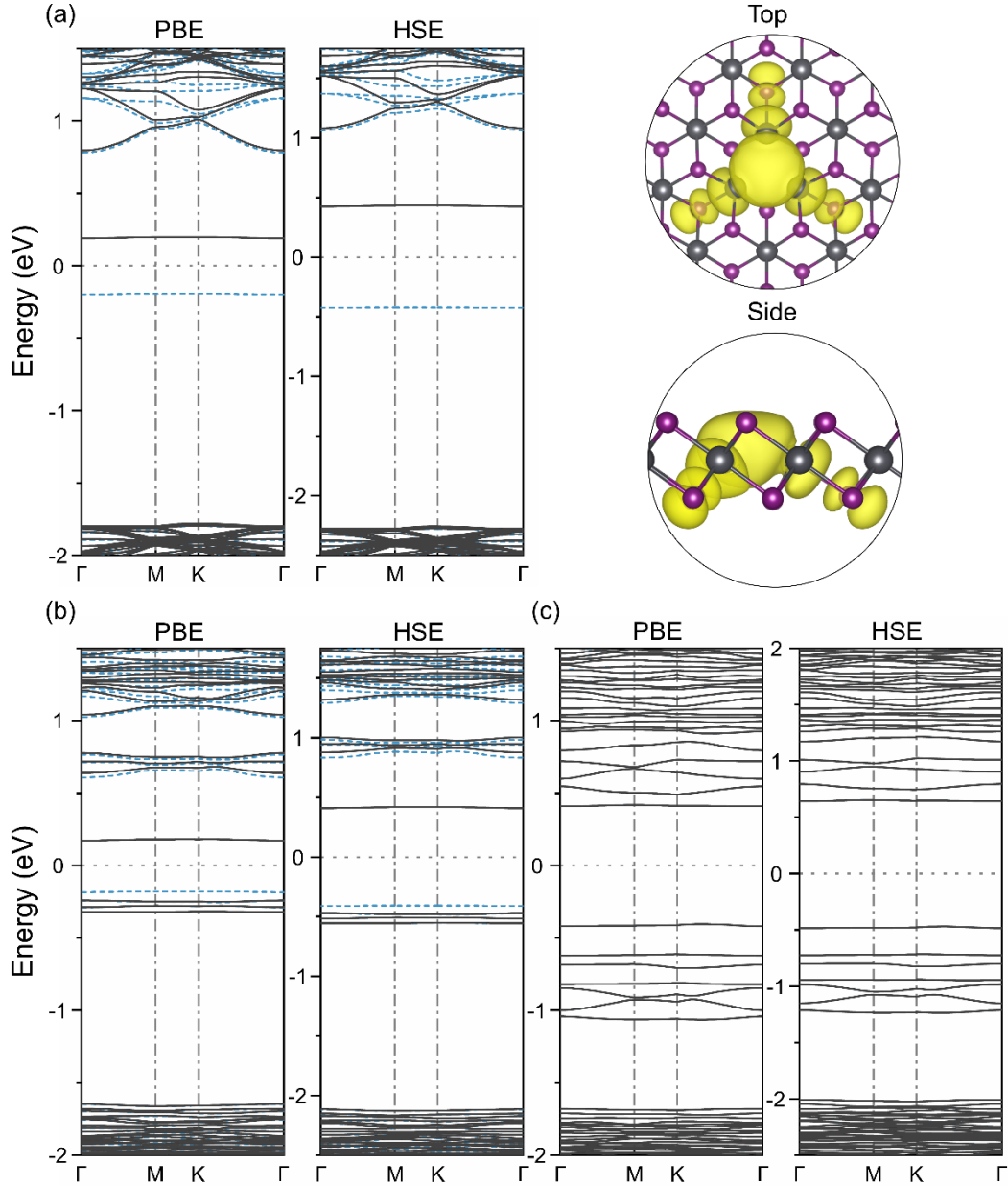


Figure 3. Band structures by PBE and HSE methods of ML-PbI₂ containing V_I. (a) V_{I-1}, with V_I concentration of 1.38%, (b) V_{I-2}, with V_I concentration of 9.72%, (c) V_{I-3}, with V_I concentration of 19.44%. The black solid lines represent the spin-down states and the blue dotted lines represent the spin-up states. The insets are the spatial distribution of localized defective level of V_{I-1} from top and side views.

Figure 3a-c show the band structures of defective ML-PbI₂ calculated by PBE and HSE methods. The E_g of V_{I-1} for dilute doping is 2.57 eV (PBE value) and 3.31 eV (HSE value) which are comparable with perfect ML-PbI₂. Therefore, the low concentration of V_I has no

obvious effect on the E_g . However the presence of V_I may lead to non-radiative recombination due to the in-gap defective levels. As illustrated in Fig. 3a, two spin-polarized local impurity levels are generated in the bandgap of ML-PbI₂ with the fully occupied spin-up state (blue dotted line) and empty spin-down state (black solid line). Both two flat defect states are deep levels due to their large ionization energy, around 0.60 and 0.98 eV (PBE value) and 0.65 and 1.50 eV (HSE value) below CB edge. These deep energy levels can serve as the recombination center for electrons and holes, thereby shortening the lifetime of non-equilibrium carriers. For instance, the V_{I-1} allows the release of a charged carrier of electron then forms a positive center in ML-PbI₂ thus acting as a donor impurity. The insets of Fig. 3 show the charge spatial distributions of V_{I-1} defective levels from the top and side views, where the defective states are highly localized at the three exposed Pb atoms and the V_I core, with slight contributions from the next nearest I atoms from the opposite side.

With increasing the content of iodine vacancies, corresponding to the medium-level V_{I-2} and high-level V_{I-3} , the VBs and CBs tend to shift slightly to the Fermi level (Fig. 3b and c). As expected the defective levels associated with V_I become significantly broadened. In particular, for the V_{I-3} , those empty defective levels are merged into the CBs, as indicative of a doped degenerating semiconductor, while the lower lying occupied defective bands ranging from -0.42 to -1.06 eV (PBE values) and -0.47 to -1.23 (HSE values) above VB edge. Such rich defective levels could be the sinks or reservoir of photoexcited carriers.

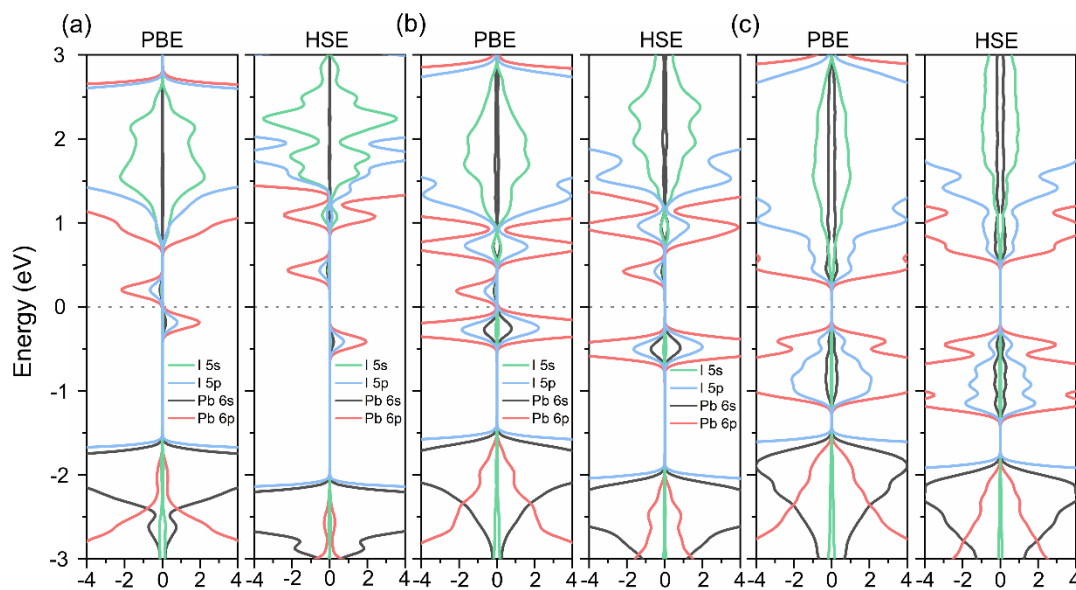


Figure 4. Comparison of the PDOS for (a) V_{I-1} , (b) V_{I-2} , and (c) V_{I-3} by PBE and HSE method, respectively. The Pb 6s orbitals is black lines, Pb 6p orbitals is red lines, I 5s orbitals is green lines, and I 5p orbitals is blue lines.

Figure 4 shows the the PDOS for the evolutions of states with the variation and distributions of vacancies. These impurity levels are mostly composed of 6p states (red lines) corresponding to the NN Pb atoms, with a smaller contribution of 5p states (blue lines) from the NN I atoms and the least for 6s states (black lines) of NN Pb atoms. As seen from Fig. 4a and b, these impurity levels near the Fermi level are localized and spin-dependent. In contrast, as shown in Fig. 4c, the impurity levels become delocalized and have no spin polarization when I-vacancy concentration increases further, developing a band-like extending defective states. One striking feature of highly V_I concentrated PbI_2 is that the defective bands, evolved from single V_I , keeps a semiconducting behavior, which is different from the metallic behavior of other 2D materials like MoS_2 ⁶⁶.

I interstitial

Next, we examined the energetics and electronic properties associated with the I_I defect. Here we only consider dilute adsorption of the iodine atom since higher uptake of iodine would lead to similar electronic and structural properties due to the large separation between each two adsorbates. As shown in Fig. 1a and b, there are two different adsorption configurations for

interstitial iodine: I_{I-I} and I_{I-Pb} . For the I_{I-I} , the adsorbing I is located and slightly tilted above the I atom in the backbone which triggers minor structural distortion on the PbI_2 below. The vertical aligned I-I bond is found with a length of 2.68 Å. For the I_{I-Pb} case, the adsorbing I atom is connected to the Pb atom in the middle layer which induces a strong lattice distortion of PbI_2 localized the anchoring site. It is obvious that the presence of interstitial I atom breaks a primitive Pb-I bond and reconstructs a Pb-I bond. A qualitative understanding of the out-of-plane displacement is that the paired electrons of the new Pb-I bond repel the electron on the I atom at the opposite side of PbI_2 . Surprisingly, the strong bond reorganization in this I_{I-Pb} has a similar E_f with that of surface adsorption in I_{I-I} . This implies again a weak bonding energy of Pb-I and explains the facile fabrication of PSCs starting from PbI_2 precursor.

The E_f of I_{I-I} and I_{I-Pb} was listed in Table 1 which is similar for these two different configurations. For I_{I-I} , the E_f is 2.56 eV (I-poor) and 0.68 eV (I-rich), and for I_{I-Pb} the values are slightly lower with 2.54 eV (I-poor) and 0.65 eV (I-rich). Therefore, compare with the Pb-rich environment, the I_I is more prone to form in I-rich condition.

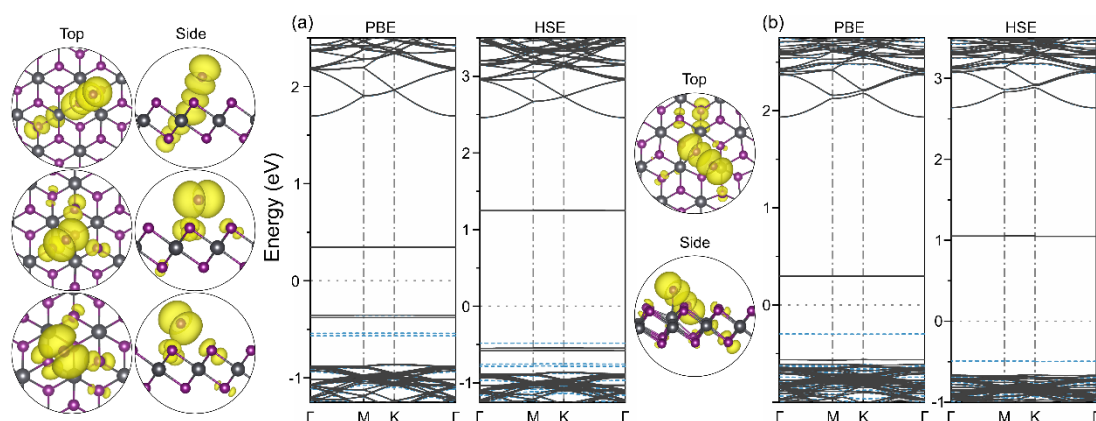


Figure 5. Band structures of (a) I_{I-I} and (b) I_{I-Pb} . The black solid lines represent the spin-down states and the blue dotted lines represent the spin-up states. The insets on the left side of the band structure show the spatial distribution of the in-gap defective states from top and side views. For the I_{I-I} , three defective charge plots are located from top to bottom according to the sequence of reducing energy level.

Figure 5 shows the band structures of I_{I-I} and I_{I-Pb} defective system. The calculated E_g of I_{I-I} are 2.55 eV for PBE and 3.30 eV for HSE whereas it are slightly different for I_{I-Pb} : 2.50 eV

for PBE and 3.29 eV for HSE. Although these values of E_g are similar to the pristine ML-PbI₂ (2.55 eV and 3.32 eV), the interstitial defects induces new characteristics with the introduced defect levels. As shown in Fig. 5a, for I_{I-I} system, six spin-polarized localized impurity levels are created in the bandgap of ML-PbI₂. The impurity levels are quite close to the VBs (locating at 0.10, 0.30 and 0.37 eV above the VB edge by HSE), indicating that the interstitial iodine gives rise to shallow acceptor levels. The iodine atom could take the electrons and become a negative center, thus acting as an acceptor impurity, which provides holes carriers in ML-PbI₂. Besides, we also notice one defect level is 2.11 eV from VBs by HSE and thus as a deep level, indicated that the I_{I-I} will induce recombination center in ML-PbI₂ as well. As shown in the inset of Fig. 5, the defective state mainly consists of 5*p* states of I atoms. These shallow impurity levels are dominated by 5*p_x* and 5*p_y* orbitals of I_{I-I} while the deep level relies on the 5*p_z* orbitals.

As for I_{I-Pb} system, the interstitial iodine atom produces two defect levels, one is an occupied and spin-up state with a shallow nature (0.16 eV above VB by HSE) and another is empty and spin down state with a relatively deep location (1.70 eV above VB by HSE), as shown in Fig. 5b. The real space representation of the state shows that it is mainly contributed by the 5*p* orbital coupling between adsorbed I atom and the I atom from the broken Pb-I bond.

Figure 6 shows the PDOS of I_{I-I} and I_{Pb-I} systems. Consistent with the real space distribution as shown in insets of Fig. 5, the I 5*p* states dominate the localized defective levels whereas the interlayer Pb atom almost have no contribution. Both two interstitial adsorptions induce shallow (near the band edge) defect energy states, which will produce relatively slow electron–hole recombination kinetics. This can be attributed to the charge defect-tolerance of PbI₂, which generally form Pb (6*s*)-I (5*p*) and Pb (6*p*)-I (5*p*) antibonding molecular orbitals. Analogously, lead-halide perovskite was found as a defect-tolerant semiconductor with lacking of bonding–antibonding interaction between the conduction bands and valence bands⁶⁷⁻⁷⁰.

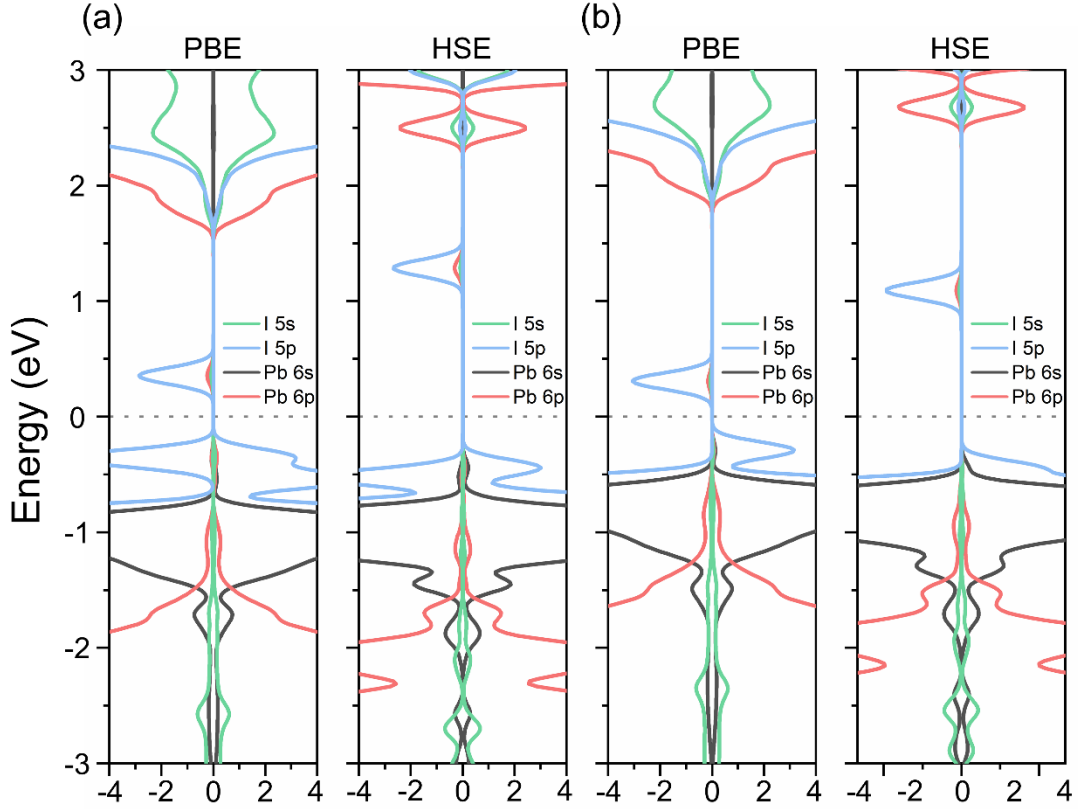


Figure 6. Comparison of the PDOS for (a) I_{I-I} and (b) I_{I-Pb} . The Pb 6s orbitals is black lines, Pb 6p orbitals is red lines, I 5s orbitals is green lines, and I 5p orbitals is blue lines.

Band alignment and implications for solar cell application

Finally we would like to analyze the band alignment between perfect and defective PbI_2 together with other common PSCs materials like the $MAPbI_3$, $FAPbI_3$ and electron hole transport materials. Figure 7 depicts the alignment of band edges, levels of point defects in PbI_2 and other CBM/VBM of $FAPbI_3$, $MAPbI_3$, TiO_2 , SnO_2 , and ZnO from literatures.^{71, 72} Figure 8 shows some possible interfaces formed between PbI_2 and $MAPbI_3$, which have the potential to create a Schottky junction between p-type PbI_2 and perovskite $MAPbI_3$. The values of work function W of the perfect and defective ML- PbI_2 system are listed in Table 1. The work function of perfect PbI_2 is 5.91 eV, which drops to 5.58 and 4.60 eV for dilute and heavy doping of vacancies, respectively. Surprisingly, the minor adsorption of interstitial iodine would reduce the W to 4.62 eV.

According to our calculations, the I_V and I_I have a very low formation energy and associated with in-gap defective levels. This means a high density of such defects is highly

probable. Our calculated band structure shows the significant broadening of the defective states which could be a band-like extending nature. Owing to its relatively big intrinsic band gap of PbI_2 , the Fermi level is less likely to cross such defective band-like states, thus the PbI_2 still remains a semiconducting state, as shown by our calculations of the high-content vacancy case of $V_{1,3}$. In principle, such rich defective levels allow the reservoir or sinks of electron/hole carriers in PbI_2 . The PbI_2 itself cannot be directly used for photo-excited carriers generation due to its poor thermodynamic stability reflected by the weak Pb-I bond. However, as an important precursor for MAPbI_3 and FAPbI_3 , remnant tiny PbI_2 is possible^{19, 20} and plays some roles in affecting the efficiency of the perovskite material. In real PSC materials, the PbI_2 could play dual roles: (1) Forming Schottky-type interface with MAPbI_3 (or FAPbI_3): Since the PbI_2 is p-type and according to our energy alignment analysis in Fig. 7, the interface would be Schottky type. Figure 8a shows the schematic diagram of Schottky junction between p-type PbI_2 and perovskite MAPbI_3 . The highly dense low-lying defective states in PbI_2 , mainly from the I_i , would raise the Fermi level and reduce the Schottky barrier. The leakage of the electrons from the FAPbI_3 or MAPbI_3 into the PbI_2 would generate the built-in potential across the interface. Such built-in potential would help to facilitate the electron-hole separation and promote the carrier lifetime. (2) Acting as traps or recombination center: As shown in Fig. 7, the high-lying defective states associated with the V_1 locate below the CBM of FAPbI_3 and MAPbI_3 which are empty and allows carriers trapping or recombination. This would reduce the carrier lifetime in the host FAPbI_3 or MAPbI_3 . Therefore, PbI_2 would play both negative and positive roles in PSCs, which have a good agreement with previous works^{20, 21, 24}. To promote the efficiency by the Schottky effect, the I_i defect is favored, and to reduce the recombination centers the V_1 defect would be suppressed.

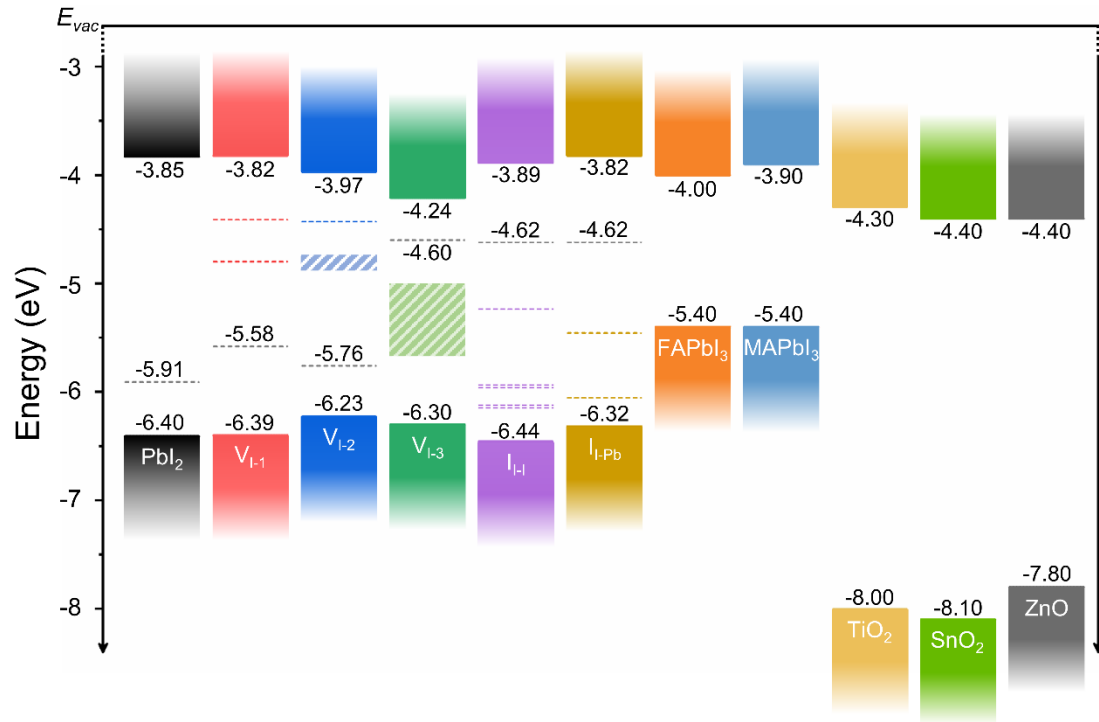


Figure 7. Band alignment of pristine and defective ML- PbI_2 according to PBE results, compared with some other materials available for PSCs. The positions of the VBM and CBM are labeled, and the defective states in the bandgap are represented with dashed lines and defective bands (for V_{I-2} and V_{I-3} cases only in the light blue and light green slashes, respectively). The levels of work function (Fermi levels relative to the E_{vac}) are plotted with dark gray dashed lines.

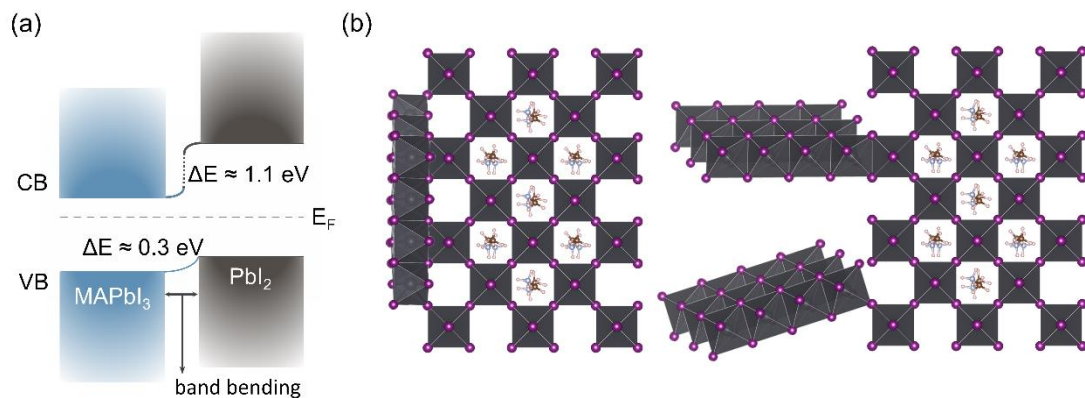


Figure 8. (a) Schematic diagram of Schottky junction between p-type PbI_2 and perovskite $MAPbI_3$. (b) Artificial illustration of interfaces formed between PbI_2 and $MAPbI_3$.

Conclusion

In summary, we have investigated the defective states in the PbI_2 for the iodine vacancies and interstitial defects by using the first-principles study. Under Pb-rich and moderate growth condition, the iodine vacancy is the dominant defect, whereas under I-rich condition, the iodine interstitial becomes more popular. A noticeable trend was the steady decrease in bandgap with the growth of iodine vacancy, due to the consistent increase in the number of defective levels. For iodine vacancy, it introduces deep levels and forms the carrier recombination center. These defective states act as trapping and scattering centers for conducting carriers and decrease their electronic mobility. For iodine interstitial, shallow trap states and deep levels are found simultaneously, which can be attributed to the charge defect-tolerance analogized to lead-halide perovskite. The low-lying defective levels in remnant PbI_2 would allow the formation of Schottky-type junction with MAPbI_3 (or FAPbI_3) which can prolong the lifetime of carriers in the perovskite due to the built-in potential. Our work sheds some lights on the dual roles of the PbI_2 and a proper defect engineering of such residual PbI_2 phase would be beneficial for the promoted efficiency of perovskite solar cells.

ASSOCIATED CONTENT

Supporting Information

Relaxed atomic structures of medium and high content of iodine vacancies. This material is available free of charge via the Internet at <http://pubs.acs.org>.

AUTHOR INFORMATION

Corresponding Author

yongqingcai@um.edu.mo

Notes

The authors declare no competing financial interests.

ACKNOWLEDGMENT

This work is supported by the University of Macau (SRG2019-00179-IAPME) and the Science and Technology Development Fund from Macau SAR (FDCT-0163/2019/A3), the Natural Science Foundation of China (Grant 22022309) and Natural Science Foundation of Guangdong Province, China (2021A1515010024). This work was performed in part at the High Performance Computing Cluster (HPCC) which is supported by Information and Communication Technology Office (ICTO) of the University of Macau.

REFERENCES

- (1) Tian, W.; Zhou, H.; Li, L. Hybrid organic–inorganic perovskite photodetectors. *Small* **2017**, 13, No. 1702107.
- (2) Yin, W. J.; Shi, T.; Yan, Y. Unique properties of halide perovskites as possible origins of the superior solar cell performance. *Adv. Mater.* **2014**, 26, 4653-4658.
- (3) Dou, L.; Yang, Y. M.; You, J.; Hong, Z.; Chang, W.-H.; Li, G.; Yang, Y. Solution-processed hybrid perovskite photodetectors with high detectivity. *Nat. Commun.* **2014**, 5, 1-6.
- (4) Green, M. A.; Dunlop, E. D.; Hohl - Ebinger, J.; Yoshita, M.; Kopidakis, N.; Hao, X. Solar cell efficiency tables (Version 58). *Prog. Photovoltaics: Research and Applications* **2021**, 29, 657-667.
- (5) Sherkar, T. S.; Momblona, C.; Gil-Escrig, L.; Ávila, J.; Sessolo, M.; Bolink, H. J.; Koster, L. J. A. Recombination in perovskite solar cells: significance of grain boundaries, interface traps, and defect ions. *ACS Energy Lett.* **2017**, 2, 1214-1222.
- (6) Yin, W. J.; Shi, T.; Yan, Y. Unusual defect physics in CH₃NH₃PbI₃ perovskite solar cell absorber. *Appl. Phys. Lett.* **2014**, 104, No. 063903.
- (7) Burschka, J.; Pellet, N.; Moon, S.-J.; Humphry-Baker, R.; Gao, P.; Nazeeruddin, M. K.; Grätzel, M. Sequential deposition as a route to high-performance perovskite-sensitized solar

- cells. *Nature* **2013**, 499, 316-319.
- (8) Chen, Q.; Zhou, H.; Hong, Z.; Luo, S.; Duan, H.-S.; Wang, H.-H.; Liu, Y.; Li, G.; Yang, Y. Planar heterojunction perovskite solar cells via vapor-assisted solution process. *J. Am. Chem. Soc.* **2014**, 136, 622-625.
- (9) Yang, S.; Zheng, Y. C.; Hou, Y.; Chen, X.; Chen, Y.; Wang, Y.; Zhao, H.; Yang, H. G. Formation mechanism of freestanding CH₃NH₃PbI₃ functional crystals: In situ transformation vs dissolution–crystallization. *Chem. Mater.* **2014**, 26, 6705-6710.
- (10) Yoshikawa, K.; Kawasaki, H.; Yoshida, W.; Irie, T.; Konishi, K.; Nakano, K.; Uto, T.; Adachi, D.; Kanematsu, M.; Uzu, H.; Yamamoto, K. Silicon heterojunction solar cell with interdigitated back contacts for a photoconversion efficiency over 26%. *Nat Energy*. **2017**, 2, No. 17032.
- (11) Zheng, X.; Chen, B.; Dai, J.; Fang, Y.; Bai, Y.; Lin, Y.; Wei, H.; Zeng, X. C.; Huang, J. Defect passivation in hybrid perovskite solar cells using quaternary ammonium halide anions and cations. *Nat Energy*. **2017**, 2, No. 17102.
- (12) Raga, S. R.; Ono, L. K.; Qi, Y. Rapid perovskite formation by CH₃NH₂ gas-induced intercalation and reaction of PbI₂. *J. Mater. Chem. A* **2016**, 4, 2494-2500.
- (13) Yi, C.; Li, X.; Luo, J.; Zakeeruddin, S. M.; Grätzel, M. Perovskite photovoltaics with outstanding performance produced by chemical conversion of bilayer mesostructured lead halide/TiO₂ films. *Adv. Mater.* **2016**, 28, 2964-2970.
- (14) Ganose, A. M.; Savory, C. N.; Scanlon, D. O. Beyond methylammonium lead iodide: prospects for the emergent field of ns² containing solar absorbers. *Chem. Commun.* **2017**, 53, 20-44.
- (15) Bi, D.; Tress, W.; Dar, M. I.; Gao, P.; Luo, J.; Renevier, C.; Schenk, K.; Abate, A.; Giordano, F.; Baena, J.-P. C. Efficient luminescent solar cells based on tailored mixed-cation perovskites. *Sci. Adv.* **2016**, 2, No. 1501170.
- (16) Roldán-Carmona, C.; Gratiá, P.; Zimmermann, I.; Grancini, G.; Gao, P.; Grätzel, M.; Nazeeruddin, M. K. High efficiency methylammonium lead triiodide perovskite solar cells: the relevance of non-stoichiometric precursors. *Energy Environ. Sci.* **2015**, 8, 3550-3556.
- (17) Kim, Y. C.; Jeon, N. J.; Noh, J. H.; Yang, W. S.; Seo, J.; Yun, J. S.; Ho - Baillie, A.; Huang, S.; Green, M. A.; Seidel, J. Beneficial effects of PbI₂ incorporated in organo - lead halide perovskite solar cells. *Adv. Energy Mater.* **2016**, 6, No. 1502104.
- (18) Shi, B.; Yao, X.; Hou, F.; Guo, S.; Li, Y.; Wei, C.; Ding, Y.; Li, Y.; Zhao, Y.; Zhang, X. Unraveling the passivation process of PbI₂ to enhance the efficiency of planar perovskite solar cells. *J. Phys. Chem. C* **2018**, 122, 21269-21276.
- (19) Wang, L.; McCleese, C.; Kovalsky, A.; Zhao, Y.; Burda, C. Femtosecond time-resolved transient absorption spectroscopy of CH₃NH₃PbI₃ perovskite films: evidence for passivation effect of PbI₂. *J. Am. Chem. Soc.* **2014**, 136, 12205-12208.
- (20) Jacobsson, T. J.; Correa-Baena, J.-P.; Halvani Anaraki, E.; Philippe, B.; Stranks, S. D.; Bouduban, M. E.; Tress, W.; Schenk, K.; Teuscher, J. I.; Moser, J.-E. Unreacted PbI₂ as a double-edged sword for enhancing the performance of perovskite solar cells. *J. Am. Chem. Soc.* **2016**, 138, 10331-10343.
- (21) Park, B.-w.; Kedem, N.; Kulbak, M.; Yang, W. S.; Jeon, N. J.; Seo, J.; Kim, G.; Kim, K. J.; Shin, T. J.; Hodes, G. Understanding how excess lead iodide precursor improves halide perovskite solar cell performance. *Nat. Commun.* **2018**, 9, 1-8.

- (22) Supasai, T.; Rujisamphan, N.; Ullrich, K.; Chemseddine, A.; Dittrich, T. Formation of a passivating $\text{CH}_3\text{NH}_3\text{PbI}_3/\text{PbI}_2$ interface during moderate heating of $\text{CH}_3\text{NH}_3\text{PbI}_3$ layers. *Appl. Phys. Lett.* **2013**, 103, No. 183906.
- (23) Tong, C.-J.; Li, L.; Liu, L.-M.; Prezhdo, O. V. Long carrier lifetimes in PbI_2 -rich perovskites rationalized by ab initio nonadiabatic molecular dynamics. *ACS Energy Lett.* **2018**, 3, 1868-1874.
- (24) Tumen - Ulzii, G.; Qin, C.; Klotz, D.; Leyden, M. R.; Wang, P.; Auffray, M.; Fujihara, T.; Matsushima, T.; Lee, J. W.; Lee, S. J. Detrimental effect of unreacted PbI_2 on the long - term stability of perovskite solar cells. *Adv. Mater.* **2020**, 32, No. 1905035.
- (25) Gähwiller, C.; Harbeke, G. Excitonic effects in the electroreflectance of lead iodide. *Phys. Rev.* **1969**, 185, No. 1141.
- (26) Schlüter, I. C.; Schlüter, M. Electronic structure and optical properties of PbI_2 . *Phys. Rev. B* **1974**, 9, No. 1652.
- (27) Zhou, M.; Duan, W.; Chen, Y.; Du, A. Single layer lead iodide: computational exploration of structural, electronic and optical properties, strain induced band modulation and the role of spin-orbital-coupling. *Nanoscale* **2015**, 7, 15168-15174.
- (28) Flahaut, E.; Sloan, J.; Friedrichs, S.; Kirkland, A. I.; Coleman, K.; Williams, V.; Hanson, N.; Hutchison, J.; Green, M. L. Crystallization of 2H and 4H PbI_2 in carbon nanotubes of varying diameters and morphologies. *Chem. Mater.* **2006**, 18, 2059-2069.
- (29) Zhang, J.; Song, T.; Zhang, Z.; Ding, K.; Huang, F.; Sun, B. Layered ultrathin PbI_2 single crystals for high sensitivity flexible photodetectors. *J. Mater. Chem. C* **2015**, 3, 4402-4406.
- (30) Liu, X.; Ha, S. T.; Zhang, Q.; de la Mata, M.; Magen, C.; Arbiol, J.; Sum, T. C.; Xiong, Q. Whispering gallery mode lasing from hexagonal shaped layered lead iodide crystals. *ACS nano* **2015**, 9, 687-695.
- (31) Street, R.; Ready, S.; Lemmi, F.; Shah, K.; Bennett, P.; Dmitriyev, Y. Electronic transport in polycrystalline PbI_2 films. *J. Appl. Phys.* **1999**, 86, 2660-2667.
- (32) Liu, B.; Zhao, W.; Ding, Z.; Verzhbitskiy, I.; Li, L.; Lu, J.; Chen, J.; Eda, G.; Loh, K. P. Engineering bandgaps of monolayer MoS_2 and WS_2 on fluoropolymer substrates by electrostatically tuned many - body effects. *Adv. Mater.* **2016**, 28, 6457-6464.
- (33) Toulouse, A. S.; Isaacoff, B. P.; Shi, G.; Matuchová, M.; Kioupakis, E.; Merlin, R. Frenkel-like Wannier-Mott excitons in few-layer PbI_2 . *Phys. Rev. B* **2015**, 91, No. 165308.
- (34) Zhong, M.; Zhang, S.; Huang, L.; You, J.; Wei, Z.; Liu, X.; Li, J. Large-scale 2D PbI_2 monolayers: experimental realization and their indirect band-gap related properties. *Nanoscale* **2017**, 9, 3736-3741.
- (35) Yagmurcukardes, M.; Peeters, F. M.; Sahin, H. Electronic and vibrational properties of PbI_2 : From bulk to monolayer. *Phys. Rev. B* **2018**, 98, No. 085431.
- (36) Cabana, L.; Ballesteros, B.; Batista, E.; Magén, C.; Arenal, R.; Oró - Solé, J.; Rurali, R.; Tobias, G. Synthesis of PbI_2 single - layered inorganic nanotubes encapsulated within carbon nanotubes. *Adv. Mater.* **2014**, 26, 2016-2021.
- (37) Zheng, W.; Zhang, Z.; Lin, R.; Xu, K.; He, J.; Huang, F. High-Crystalline 2D Layered PbI_2 with Ultrasoft Surface: Liquid - Phase Synthesis and Application of High - Speed Photon Detection. *Adv. Electron. Mater.* **2016**, 2(11), No. 1600291.
- (38) Wang, Y.; Gan, L.; Chen, J.; Yang, R.; Zhai, T. Achieving highly uniform two-dimensional PbI_2 flakes for photodetectors via space confined physical vapor deposition. *Sci. Bull.* **2017**, 62,

1654-1662.

(39) Ghoshal, D.; Shang, H.; Sun, X.; Wen, X.; Chen, D.; Wang, T.; Lu, Z.; Gupta, T.; Efstathiadis, H.; West, D. Orientation-Controlled Large-Area Epitaxial PbI₂ Thin Films with Tunable Optical Properties. *ACS Appl. Mater. Interfaces* **2021**, 13, 32450-32460.

(40) Fan, Q.; Huang, J.; Dong, N.; Hong, S.; Yan, C.; Liu, Y.; Qiu, J.; Wang, J.; Sun, Z. Liquid exfoliation of two-dimensional PbI₂ nanosheets for ultrafast photonics. *ACS Photonics* **2019**, 6, 1051-1057.

(41) Zhong, M.; Huang, L.; Deng, H.-X.; Wang, X.; Li, B.; Wei, Z.; Li, J. Flexible photodetectors based on phase dependent PbI₂ single crystals. *J. Mater. Chem. C* **2016**, 4, 6492-6499.

(42) Han, M.; Sun, J.; Bian, L.; Wang, Z.; Zhang, L.; Yin, Y.; Gao, Z.; Li, F.; Xin, Q.; He, L. Two-step vapor deposition of self-catalyzed large-size PbI₂ nanobelts for high-performance photodetectors. *J. Mater. Chem. C* **2018**, 6, 5746-5753.

(43) Tan, M.; Hu, C.; Lan, Y.; Khan, J.; Deng, H.; Yang, X.; Wang, P.; Yu, X.; Lai, J.; Song, H. 2D lead dihalides for high - performance ultraviolet photodetectors and their detection mechanism investigation. *Small* **2017**, 13, No. 1702024.

(44) Tan, A. C.; Wright, G. A. The anodic formation of lead iodide. Evidence for the underpotential deposition of a reversible monolayer. *Ber. Bunsenges. Physik. Chem.* **1987**, 91, 341-344.

(45) Wang, H.; Wang, Z.; Yang, Z.; Xu, Y.; Ding, Y.; Tan, L.; Yi, C.; Zhang, Z.; Meng, K.; Chen, G. Ligand - Modulated Excess PbI₂ Nanosheets for Highly Efficient and Stable Perovskite Solar Cells. *Adv. Mater.* **2020**, 32(21), No. 2000865.

(46) Peng, B.; Mei, H.; Zhang, H.; Shao, H.; Xu, K.; Ni, G.; Jin, Q.; Soukoulis, C. M.; Zhu, H. High thermoelectric efficiency in monolayer PbI₂ from 300 K to 900 K. *Inorg. Chem. Front.* **2019**, 6, 920-928.

(47) Sun, Y.; Zhou, Z.; Huang, Z.; Wu, J.; Zhou, L.; Cheng, Y.; Liu, J.; Zhu, C.; Yu, M.; Yu, P. Band structure engineering of interfacial semiconductors based on atomically thin lead iodide crystals. *Adv. Mater.* **2019**, 31, No. 1806562.

(48) Sinha, S.; Zhu, T.; France-Lanord, A.; Sheng, Y.; Grossman, J. C.; Porfyrakis, K.; Warner, J. H. Atomic structure and defect dynamics of monolayer lead iodide nanodisks with epitaxial alignment on graphene. *Nat. Commun.* **2020**, 11, 1-13.

(49) Lordi, V.; Erhart, P.; Åberg, D. Charge carrier scattering by defects in semiconductors. *Phys. Rev. B* **2010**, 81, No. 235204.

(50) Zhou, W.; Fu, H. Defect-mediated electron-hole separation in semiconductor photocatalysis. *Inorg. Chem. Front.* **2018**, 5, 1240-1254.

(51) Bai, S.; Zhang, N.; Gao, C.; Xiong, Y. Defect engineering in photocatalytic materials. *Nano Energy* **2018**, 53, 296-336.

(52) Wang, S.; Jiang, Y.; Juarez-Perez, E. J.; Ono, L. K.; Qi, Y. Accelerated degradation of methylammonium lead iodide perovskites induced by exposure to iodine vapour. *Nat. Energy* **2016**, 2, 1-8.

(53) Zhang, L.; Sit, P. H.-L. Ab initio study of the role of iodine in the degradation of CH₃NH₃PbI₃. *J. Mater. Chem. A* **2017**, 5, 23976-23986.

(54) Wang, Y.; Xu, C.; Zhang, J.; Du, X.; Yan, Y. Electronic band structure and magnetic properties of I vacancy and nonmetallic atoms doped single layer PbI₂. *J. Magn. Magn. Mater.*

2018, 463, 36-43.

- (55) Kresse, G.; Furthmüller, J. Efficient iterative schemes for ab initio total-energy calculations using a plane-wave basis set. *Phys. Rev. B* **1996**, 54, No. 11169.
- (56) Kresse, G.; Furthmüller, J. Efficiency of ab-initio total energy calculations for metals and semiconductors using a plane-wave basis set. *Comput. Mater. Sci.* **1996**, 6, 15-50.
- (57) Blöchl, P. E. Projector augmented-wave method. *Phys. Rev. B* **1994**, 50, No. 17953.
- (58) Perdew, J. P.; Burke, K.; Ernzerhof, M. Generalized gradient approximation made simple. *Phys. Rev. Lett.* **1996**, 77(18), No. 3865.
- (59) Heyd, J.; Scuseria, G. E.; Ernzerhof, M. Hybrid functionals based on a screened Coulomb potential. *J. Chem. Phys.* **2003**, 118, 8207-8215.
- (60) Grimme, S.; Antony, J.; Ehrlich, S.; Krieg, H. A consistent and accurate ab initio parametrization of density functional dispersion correction (DFT-D) for the 94 elements H-Pu. *J. Chem. Phys.* **2010**, 132, No. 154104.
- (61) Wang, H.; Wang, X.; Li, D. Defects of monolayer PbI₂: a computational study. *Phys. Chem. Chem. Phys.* **2021**, 23, 20553-20559.
- (62) Kripalani, D. R.; Cai, Y.; Xue, M.; Zhou, K. Metastable interlayer Frenkel pair defects in black phosphorus. *Phys. Rev. B.* **2019**, 100, No. 224107.
- (63) Kripalani, D. R.; Sun, P. P.; Lin, P.; Xue, M.; Zhou, K. Vacancies and dopants in two-dimensional tin monoxide: An ab initio study. *Appl. Surf. Sci.* **2021**, 538, No. 147988.
- (64) Komsa, H.-P.; Kotakoski, J.; Kurasch, S.; Lehtinen, O.; Kaiser, U.; Krasheninnikov, A. V. Two-Dimensional Transition Metal Dichalcogenides under Electron Irradiation: Defect Production and Doping. *Phys. Rev. Lett.* **2012**, 109, No. 035503.
- (65) Cai, Y.; Ke, Q.; Zhang, G.; Yakobson, B. I.; Zhang, Y.-W. Highly itinerant atomic vacancies in phosphorene. *J. Am. Chem. Soc.* **2016**, 138, 10199-10206.
- (66) Zhou, W.; Dong, L.; Tan, L.; Tang, Q. First-principles study of sulfur vacancy concentration effect on the electronic structures and hydrogen evolution reaction of MoS₂. *Nanotechnology* **2021**, 32(14), No. 145718.
- (67) Brandt, R. E.; Stevanović, V.; Ginley, D. S.; Buonassisi, T. Identifying defect-tolerant semiconductors with high minority-carrier lifetimes: beyond hybrid lead halide perovskites. *MRS Commun.* **2015**, 5, 265-275.
- (68) Brandt, R. E.; Poindexter, J. R.; Gorai, P.; Kurchin, R. C.; Hoye, R. L.; Nienhaus, L.; Wilson, M. W.; Polizzotti, J. A.; Sereika, R.; Zaltauskas, R. Searching for “defect-tolerant” photovoltaic materials: combined theoretical and experimental screening. *Chem. Mater.* **2017**, 29, 4667-4674.
- (69) Kang, J.; Wang, L.-W. High defect tolerance in lead halide perovskite CsPbBr₃. *J. Phys. Chem. Lett.* **2017**, 8, 489-493.
- (70) Das, B.; Liu, Z.; Aguilera, I.; Rau, U.; Kirchartz, T. Defect tolerant device geometries for lead-halide perovskites. *Mater. Adv.* **2021**, 2, 3655-3670.
- (71) Chueh C. C.; Li, C. Z.; Jen, A. K. Y. Recent progress and perspective in solution-processed Interfacial materials for efficient and stable polymer and organometal perovskite solar cells. *Energy Environ. Sci.* **2015**, 8, 1160-1189.
- (72) Sun, P. P.; Kripalani, D. R.; Bai, L.; Chi, W.; and Zhou, K. Pentadiamond: A Highly Efficient Electron Transport Layer for Perovskite Solar Cells. *J. Phys. Chem. C.* **2021**, 125, 9, 5372–5379.

